An Open-end Transformer-based Power Tap for Interconnection of AC/DC Micro-grids

Y. Liu, J. H. Zheng, K. Shi, L. Jiang, K. Ni, Q. H. Wu

Abstract

This paper proposes an open-end transformer-based power tap (OETPT) for the interconnection of the AC sub-grid and the DC sub-grid of a hybrid micro-grid. Two topologies, Topology-A and Topology-B, were designed for OETPT, in which the primary or the secondary windings of the transformer of OETPT are grounded, respectively. Steady-state and dynamic models were developed for OETPT, based on which a vector control system was designed for the coordinated control of OETPT with Topology-A and Topology-B, respectively. OETPT achieves the decoupled control of the active and reactive powers. Simulation studies and experimental validations were undertaken to manifest the coordinated power flow control performance of OETPT with Topology-A and Topology-B, respectively.

I. Introduction

Hybrid micro-grids are state-of-the-art integration and management systems of distributed power sources and loads [1]-[3]. In a hybrid micro-grid illustrated in Fig. 1 (a), the interface between the AC sub-grid and the DC sub-grid consists of parallel connected AC/DC converters and transformers [4]-[6]. The parallel connection topology can provide high power density and current capacity for the power exchange between the AC sub-grid and the DC sub-grid [7],[8]. The AC/DC interface plays an importance role in the power flow control, power quality regulation, and stability control of the entire micro-grid [9]-[11]. As the increase of copper price and the decrease of the cost of semiconductor devices, it is desirable to use less transformers and more power electronics converters in the AC/DC interface of micro-grids [12]-[14].

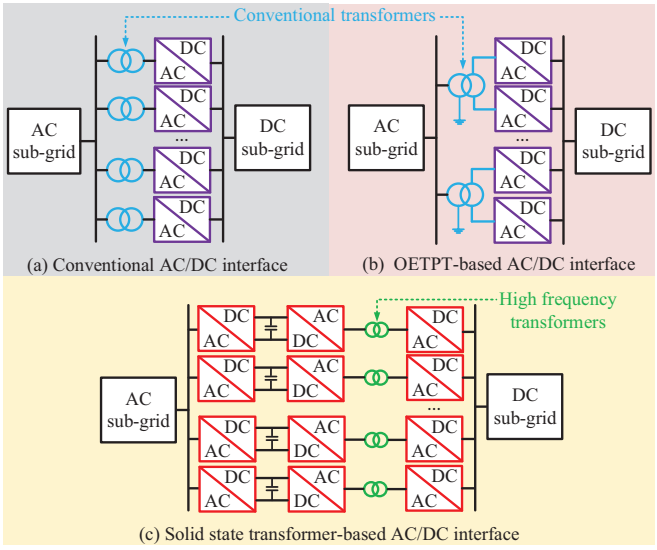

Fig. 1. Three AC/DC interfaces for hybrid micro-grids.

The solid state transformer was first proposed in 1970 [15]. High frequency converter links were implemented on the primary and the secondary windings of a transformer such that the volume of the transformer was reduced and its operating efficiency was improved [16]. As such, the solid state transformer was employed as the AC/DC interface of hybrid micro-grids in [17],[18], the topology of which is illustrated in Fig. 1 (c). Recent studies of the solid state transformer mainly focused on the topology design of the high frequency links, such as the modular multilevel converter topology designed in [19], the AC-AC active H-bridge topology proposed in [12], and the high-voltage device-based high frequency links designed in [20]. Compared with the conventional transformer, the solid state transformer not only has the voltage transformation and current isolation functions, but also offers more flexibility in power flow control, power quality regulation, and fault limitation [17]. Nevertheless, the solid state transformer contains a large number of switching devices, which significantly complicate its control system, as well as the hardware design and the practical implementation [17]. Moreover, the complex structure of a solid state transformer weakens its reliability.

Besides the conventional interface and the solid-state transformer-based interface, the existing studies have also presented various interface topologies according to their different control objectives. A two-stage converter configuration was proposed

in [21] for storage integration. The energy storage was connected on the DC bus between a DC/DC and a DC/AC converter to coordinate the power generation of renewable power sources. Nevertheless, energy storages devices are more desirable to be installed along with the distributed power sources to achieve flexible local coordination of the active power. [22] and [23] proposed a hierarchical-structured topology for the connection of hybrid micro-grids, in which DC micro-grids and AC micro-grids were connected in parallel or series according to their voltage levels. The disadvantage of such topology lies in that it has limited flexibility and freedom in synthesizing the location and voltage level of micro-grids.

To fill the gap between the conventional interface and the solid state transformer-based interface, this paper proposes an OETPT for the AC/DC interface of a hybrid micro-gird, the schematic of which is shown in Fig. 1 (b). The AC sub-grid is connected with the secondary-side of conventional transformers, and the primary-side of transformers are open-end and two terminals of primary windings are connected with two two-level AC/DC converters. This topology with secondary windings of transformers grounded is referred to as Topology-A of OETPT. Another topology (Topology-B) with primary windings of transformers grounded was designed for OETPT as well in this paper. OETPT is built with off-the-shelf components of the conventional interface of a micro-grid, i.e., the components of conventional transformers and two-level AC/DC converters. OETPT represents a novel open-end operation topology of the conventional components. OETPT not only inherits the simple structure and the voltage transformation and current isolation capabilities of a conventional interface, but also possesses the power flow control and power quality regulation functions of a solid state transformer-based interface. Compared with the conventional interface, the OETPT-based interface requires only half number of transformers, which significantly reduces the cost of a hybrid micro-grid.

The open-end operation of transformers was previously studied in [24], in which an inductor was integrated in the open-end transformer to limit the circulating current between parallel connected converters. [25] designed a LCL filter for the harmonic cancelation of the open-end transformer proposed in [24]. Regarding the case of the AC/DC interface of micro-grids, the key objectives are to control the active power flowing between AC and DC sub-grids as well as the reactive power flowing into the AC sub-grid, which were not investigated in [24],[25]. Therefore, this paper mainly focuses on the open-end operation of OETPT and its power flow control function, which covers topology design, circuit analysis, control system design, as well as simulation and experiment validation.

The control of AC/DC hybrid micro-grids is mainly realized with the droop control-based methods. The droop control-based methods are applied in the frequency control of AC sub-grids [26], the DC voltage regulation of DC sub-grids [27], as well as the AC voltage control of AC sub-grids [28]. Droop control-based methods have shown merits in aspects of simple structure, mature design techniques, and easy to implement in practice. For appropriate power sharing between parallel-connected converters in hybrid micro-grids, studies [29], [30] were carried out to investigate the coordination of droop coefficients of droop controllers. The virtual synchronous generator technique is another kind of power sharing control method in the study of hybrid micro-grids [31]. The basic idea of the virtual synchronous generator controller is to implement the equations of motion of a synchronous generator in the power control loops of converter, thereby achieving proper power sharing and inertia response between parallel-connected converters. Analogously, the virtual impedance control scheme was proposed to eliminate circulating current arising from parallel connected converters [32], through inserting a virtual impedance in the current control loops of converters.

According to the above, mature control technologies are available for various control objectives of hybrid micro-grids. Hence, the power management and stability control of micro-grids are not the focus of this paper. This paper primarily focus on novel topology design for the interfaces of AC sub-grids and DC sub-grids in a hybrid micro-grid. Overall, the main contributions of this paper are summarized as follows. Two kinds of topologies of OETPT, i.e., Topology-A and Topology-B, are designed for the flexible power flow control between the AC and DC sub-grids of hybrid micro-grids. The decoupled power flow controllers are designed for OETPT with Topology-A and Topology-B, respectively. Moreover, simulation studies are carried out considering the normal operation conditions, grid unbalance operation conditions, and earth fault conditions of micro-grids to investigate the power flow control performance of OETPT. Experimental validations are undertaken to validate feasibility of OETPT with Topology-A and Topology-B as well.

Section II presents the topology design and circuit analysis of OETPT. Two topologies, Topology-A and Topology-B, are designed for OETPT. In Topology-A, the primary windings of OETPT are open-end and the secondary windings are grounded. In Topology-B, the primary windings of OETPT are grounded, while the secondary windings are open-end. The equivalent circuits and power flow distribution of OETPT are analyzed in Section II as well. Section III is dedicated to the control system design of OETPT. Dynamic models of OETPT with Topology-A and Topology-B are investigated, based on which a vector control system is design for the decoupled active and reactive power control of Topology-A and Topology-B, respectively. The power flow control performances of OETPT with Topology-A and Topology-B respectively are studied in Section IV through simulations. Experimental validations are undertaken in Section V thereafter. According to the simulation and experiment results, discussions and conclusions are draw in Section VII.

II. Topology Design and Circuit Analysis of OETPT

An OETPT is made up of a three-phase transformer and two two-level AC/DC converters. According to the requirement on the position of the grounding point, two topologies were designed for OETPT.

A. Topology-A: Grounding Point is Required at the Secondary-side of OETPT

In Topology-A, a two-level AC/DC converter is connected to two terminals of primary windings of the three-phase transformer through an RL filter, respectively, as illustrated in Fig. 2 (a). Two two-level converters are referred to as bridge 1 and bridge 2, respectively. Dot ends of secondary windings of the transformer are connected with the AC sub-grid, and un-dot ends of secondary windings are grounded, as presented in Fig. 2 (a), where P_1 and Q_1 are active and reactive power outputs of bridge 1, P_2 and Q_2 are active and reactive power outputs of bridge 2, and P_3 and Q_3 are the active and reactive power transferred to the AC sub-grid.

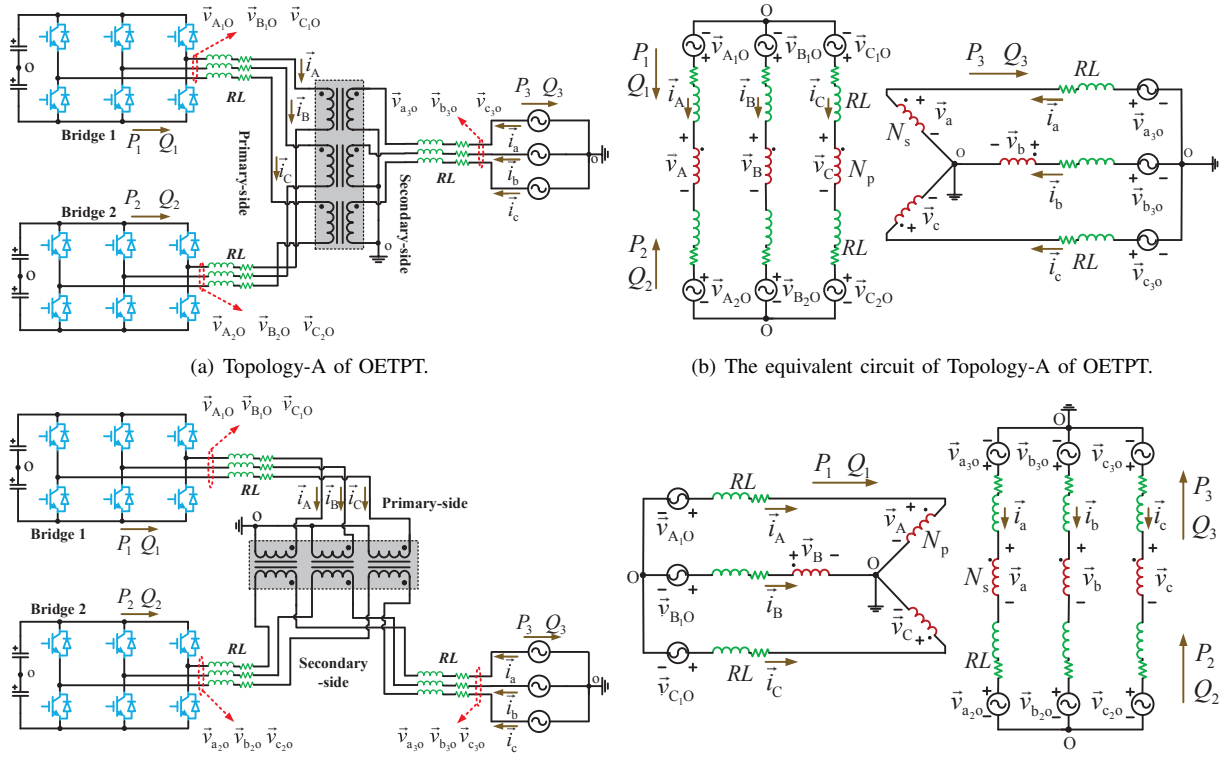

(a) Topology-A of OETPT.

(b) The equivalent circuit of Topology-A of OETPT.

(c) Topology-B of OETPT.

(d) The equivalent circuit of Topology-B of OETPT.

Fig. 2. Topology-A and Topology-B of OETPT and their equivalent circuits.

The equivalent circuit of Topology-A of OETPT is as presented in Fig. 2 (b), where $\overrightarrow{v}_{\mathrm{A_1O}}$, $\overrightarrow{v}_{\mathrm{B_1O}}$, and $\overrightarrow{v}_{\mathrm{C_1O}}$ are voltage outputs of phase A, B, and C of bridge 1, respectively, $\overrightarrow{v}_{\mathrm{A_2O}}$, $\overrightarrow{v}_{\mathrm{B_2O}}$, and $\overrightarrow{v}_{\mathrm{C_2O}}$ are voltage outputs of phase A, B, and C of bridge 2, and $\overrightarrow{v}_{\mathrm{a_3o}}$, $\overrightarrow{v}_{\mathrm{b_3o}}$, and $\overrightarrow{v}_{\mathrm{c_3o}}$ are the voltage of phase A, B, and C of the secondary-side AC sub-grid. Moreover, the primary- and secondary-side three-phase voltage and current of the transformer satisfy

$$\begin{cases} \dfrac{v_{\mathrm{A}}}{v_{\mathrm{a}}} \approx \dfrac{v_{\mathrm{A_1O}} - v_{\mathrm{A_2O}}}{v_{\mathrm{a_3o}}} = \dfrac{N_{\mathrm{p}}}{N_{\mathrm{s}}} = k \\ \dfrac{v_{\mathrm{B}}}{v_{\mathrm{b}}} \approx \dfrac{v_{\mathrm{B_1O}} - v_{\mathrm{B_2O}}}{v_{\mathrm{b_3o}}} = k \\ \dfrac{v_{\mathrm{C}}}{v_{\mathrm{c}}} \approx \dfrac{v_{\mathrm{C_1O}} - v_{\mathrm{C_2O}}}{v_{\mathrm{c_3o}}} = k = \dfrac{i_{\mathrm{a}}}{i_{\mathrm{A}}} \end{cases} \tag{1}$$

where N_{p} and N_{s} denote the turns number of primary and secondary windings of the transformer, respectively, k denotes the turns ratio, v_{A} and v_{a} are the voltage of dot ends of primary and secondary windings with respect to the corresponding un-dot ends, respectively, and i_{A} and i_{a} represent the current flowing through primary and secondary windings of the transformer, respectively. v_{B}, v_{b}, i_{B}, i_{b}, v_{C}, v_{c}, i_{C}, and i_{c} represent the voltage and the current of phase B and phase C, respectively. Neglecting the losses on leakage impedances of the transformer and filter impedances and assuming that OETPT is operating under balanced load conditions, the power transferred from the primary-side to the secondary-side of OETPT is

$$S = 3\overrightarrow{v}_{\mathrm{A_1A_2}}\overrightarrow{i}^{\,*}_{\mathrm{A}} = 3(\overrightarrow{v}_{\mathrm{A_1O}} - \overrightarrow{v}_{\mathrm{A_2O}})\overrightarrow{i}^{\,*}_{\mathrm{A}} = 3\overrightarrow{v}_{\mathrm{a_3o}}\overrightarrow{i}^{\,*}_{\mathrm{a}} \tag{2}$$

where $\overrightarrow{i}^{\,*}_{\mathrm{A}}$ denotes the conjugated vector of $\overrightarrow{i}_{\mathrm{A}}$. According to (2), on condition that $\overrightarrow{v}_{\mathrm{A_1O}} = -\overrightarrow{v}_{\mathrm{A_2O}}$, bridge 1 and bridge 2 generate the same amount of active and reactive power to the secondary-side of OETPT.

B. Topology-B: Grounding Point is Required at the Primary-side of OETPT

In Topology-B, a two-level converter is connected to dot ends of primary windings of the transformer, which is referred to as bridge 1 as illustrated in Fig. 2 (c). The un-dot ends of primary windings are grounded. Another two-level converter is connected to un-dot ends of secondary windings of the transformer. Dot ends of secondary windings are connected with the AC sub-grid.

The equivalent circuit of Topology-B is as shown in Fig. 2 (d), where $\overrightarrow{v}_{\mathrm{a_2o}}$, $\overrightarrow{v}_{\mathrm{b_2o}}$, and $\overrightarrow{v}_{\mathrm{c_2o}}$ are voltage outputs of phase A, B, and C of bridge 2, $\overrightarrow{v}_{\mathrm{a_3o}}$, $\overrightarrow{v}_{\mathrm{b_3o}}$, and $\overrightarrow{v}_{\mathrm{c_3o}}$ are the voltage of phase A, B, and C of the AC sub-grid. The three-phase voltage and current on the primary- and secondary-side of OETPT satisfy

$$\begin{cases} \dfrac{v_{\mathrm{A}}}{v_{\mathrm{a}}} \approx \dfrac{v_{\mathrm{A_1O}}}{v_{\mathrm{a_3o}} - v_{\mathrm{a_2o}}} = k \\ \dfrac{v_{\mathrm{B}}}{v_{\mathrm{b}}} \approx \dfrac{v_{\mathrm{B_1O}}}{v_{\mathrm{b_3o}} - v_{\mathrm{b_2o}}} = k \\ \dfrac{v_{\mathrm{C}}}{v_{\mathrm{c}}} \approx \dfrac{v_{\mathrm{C_1O}}}{v_{\mathrm{c_3o}} - v_{\mathrm{c_2o}}} = k = \dfrac{i_{\mathrm{a}}}{i_{\mathrm{A}}} \end{cases} \tag{3}$$

Neglecting losses on transformer leakage impedances and filter impedances and assuming that the DC sub-grid and AC sub-grid are operating under balanced load conditions, the power transferred from the primary-side to the secondary-side of OETPT is

$$S_1 = 3\overrightarrow{v}_{\mathrm{A_1O}}\overrightarrow{i}^{\,*}_{\mathrm{A}} \tag{4}$$

The power transferred from bridge 2 to the AC sub-grid is

$$S_2 = -3\overrightarrow{v}_{\mathrm{a_2o}}\overrightarrow{i}^{\,*}_{\mathrm{a}} \tag{5}$$

Then the power transmitted from the DC sub-grid to the AC sub-grid is

$$S = S_1 + S_2 = 3\overrightarrow{v}_{\mathrm{A_1O}}\overrightarrow{i}^{\,*}_{\mathrm{A}} - 3\overrightarrow{v}_{\mathrm{a_2o}}\overrightarrow{i}^{\,*}_{\mathrm{a}} = 3\overrightarrow{v}_{\mathrm{a_3o}}\overrightarrow{i}^{\,*}_{\mathrm{a}} \tag{6}$$

III. Control Systems Design of OETPT

For the flexible control of the active and reactive power flowing between the AC sub-grid and the DC sub-grid, a vector control system was designed for OETPT with Topology-A and Topology-B, respectively.

A. Dynamic Models of OETPT

1. Dynamic Model of Topology-A of OETPT:

Referring to Fig. 2, the dynamics of bridge 1 and its RL filter can be described in per unit form with

$$\begin{cases} 2L_{\mathrm{s}}\dfrac{di_{\mathrm{A}}}{dt} = v_{\mathrm{A_1O}} - 2R_{\mathrm{s}}i_{\mathrm{A}} - v_{\mathrm{a_3o}} \\ 2L_{\mathrm{s}}\dfrac{di_{\mathrm{B}}}{dt} = v_{\mathrm{B_1O}} - 2R_{\mathrm{s}}i_{\mathrm{B}} - v_{\mathrm{b_3o}} \\ 2L_{\mathrm{s}}\dfrac{di_{\mathrm{C}}}{dt} = v_{\mathrm{C_1O}} - 2R_{\mathrm{s}}i_{\mathrm{C}} - v_{\mathrm{c_3o}} \end{cases} \tag{7}$$

where the primary-side of the transformer adopts the generator convention and the secondary-side adopts the motor convention. By applying the dq-reference frame, (7) can be rewritten in dq-reference frame as [33],[34]

$$\begin{cases} \dfrac{di_{\mathrm{d_1}}}{dt} = \dfrac{1}{2L_{\mathrm{s}}}(-2R_{\mathrm{s}}i_{\mathrm{d_1}} + 2\omega_{\mathrm{s}}L_{\mathrm{s}}i_{\mathrm{q_1}} + v_{\mathrm{d_1}} - v_{\mathrm{d_3}}) \\ \dfrac{di_{\mathrm{q_1}}}{dt} = \dfrac{1}{2L_{\mathrm{s}}}(-2R_{\mathrm{s}}i_{\mathrm{q_1}} - 2\omega_{\mathrm{s}}L_{\mathrm{s}}i_{\mathrm{d_1}} + v_{\mathrm{q_1}} - v_{\mathrm{q_3}}) \end{cases} \tag{8}$$

where ω_{s} denotes the frequency of the AC sub-grid, $i_{\mathrm{d_1}}$ and $i_{\mathrm{q_1}}$ are the d- and q-axis components of i_{A}, i_{B}, and i_{C}, $v_{\mathrm{d_1}}$ and $v_{\mathrm{q_1}}$ are the d- and q-axis components of $v_{\mathrm{A_1O}}$, $v_{\mathrm{B_1O}}$, and $v_{\mathrm{C_1O}}$, and $v_{\mathrm{d_3}}$ and $v_{\mathrm{q_3}}$ are the d- and q-axis components of $v_{\mathrm{a_3o}}$, $v_{\mathrm{b_3o}}$, and $v_{\mathrm{c_3o}}$. The dynamics of bridge 2 and its RL filter can be modelled analogously with (8).

2. Dynamic Model of Topology-B of OETPT:

Referring to Fig. 2, the dynamics of bridge 2 and its RL filter in Topology-B can be modelled in per unit form as

$$\begin{cases} 2L_{\mathrm{s}}\dfrac{di_{\mathrm{a}}}{dt} = v_{\mathrm{a_2o}} - 2R_{\mathrm{s}}i_{\mathrm{a}} + v_{\mathrm{A_1O}} - v_{\mathrm{a_3o}} \\ 2L_{\mathrm{s}}\dfrac{di_{\mathrm{b}}}{dt} = v_{\mathrm{b_2o}} - 2R_{\mathrm{s}}i_{\mathrm{b}} + v_{\mathrm{B_1O}} - v_{\mathrm{b_3o}} \\ 2L_{\mathrm{s}}\dfrac{di_{\mathrm{c}}}{dt} = v_{\mathrm{c_2o}} - 2R_{\mathrm{s}}i_{\mathrm{c}} + v_{\mathrm{C_1O}} - v_{\mathrm{c_3o}} \end{cases} \tag{9}$$

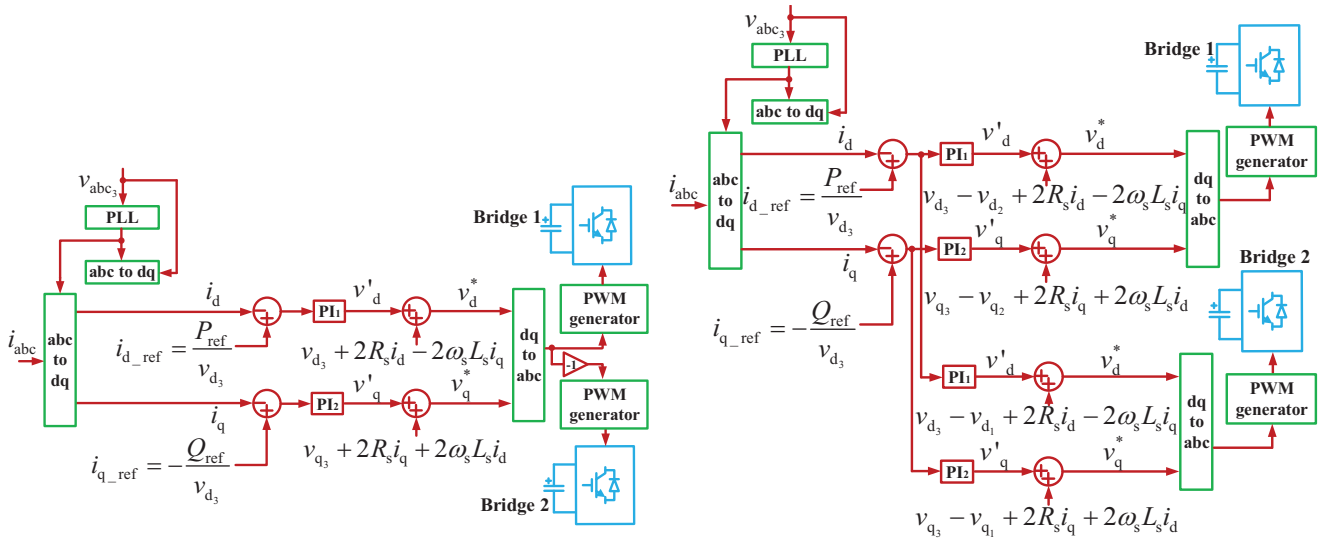

(a) The vector control system of OETPT with Topology-A.

(b) The vector control system of OETPT with Topology-B.

Fig. 3. The vector control system of OETPT with Topology-A and Topology-B.

where bridge 2 uses the generator convention and the AC sub-grid employs the motor convention. In the dq-reference frame, (9) can be rewritten as [33],[34]

$$\begin{cases} \dfrac{di_{\mathrm{d}_2}}{dt} = \dfrac{1}{2L_{\mathrm{s}}}[-2R_{\mathrm{s}}i_{\mathrm{d}_2} + 2\omega_{\mathrm{s}}L_{\mathrm{s}}i_{\mathrm{q}_2} + v_{\mathrm{d}_2} - (v_{\mathrm{d}_3} - v_{\mathrm{d}_1})] \\ \dfrac{di_{\mathrm{q}_2}}{dt} = \dfrac{1}{2L_{\mathrm{s}}}[-2R_{\mathrm{s}}i_{\mathrm{q}_2} - 2\omega_{\mathrm{s}}L_{\mathrm{s}}i_{\mathrm{d}_2} + v_{\mathrm{q}_2} - (v_{\mathrm{q}_3} - v_{\mathrm{q}_1})] \end{cases} \tag{10}$$

where i_{d_2} and i_{q_2} are the d- and q-axis components of i_{a}, i_{b}, and i_{c}, and v_{d_2} and v_{q_2} are the d- and q-axis components of $v_{\mathrm{a}_2\mathrm{o}}$, $v_{\mathrm{b}_2\mathrm{o}}$, and $v_{\mathrm{c}_2\mathrm{o}}$. The dynamics of bridge 1 and its RL filter in Topology-B is similar with (10).

B. Vector Control Systems Designed for OETPT

1. Vector Control System for Topology-A:

Based on the dynamic model (8) expressed in the dq reference frame, a vector control system was designed for OETPT with Topology-A as depicted in Fig. 3 (a), which realizes the decoupled control of the active and reactive power flowing through OETPT. The active power is controlled by regulating the d-axis current flowing into the AC sub-grid. The q-axis current is controlled to regulated the reactive power flowing into the AC sub-grid. A two-loop configuration is adopted in the vector control system. The inner control loops are for the regulation of the d- and q-axis current, respectively. The outer control loops are for the control of active power and reactive power, respectively. Within Fig. 3 (a), P_{ref} is the reference of the active power transferred to the secondary-side of OETPT, Q_{ref} denotes the reactive power reference, $v_{\mathrm{d}_3} + 2R_{\mathrm{s}}i_{\mathrm{d}} - 2\omega_{\mathrm{s}}L_{\mathrm{s}}i_{\mathrm{q}}$ and $v_{\mathrm{q}_3} + 2R_{\mathrm{s}}i_{\mathrm{q}} + 2\omega_{\mathrm{s}}L_{\mathrm{s}}i_{\mathrm{d}}$ are feed-forward compensation terms, and $\mathrm{PI}_i (i = 1, 2)$ are proportion-integration (PI) controllers.

In the dq reference frame, the active and reactive power transferred to the AC sub-grid are $P_3 = v_{\mathrm{d}_3}i_{\mathrm{d}} + v_{\mathrm{q}_3}i_{\mathrm{q}}$ and $Q_3 = v_{\mathrm{q}_3}i_{\mathrm{d}} - v_{\mathrm{d}_3}i_{\mathrm{q}}$, respectively. Aligning the d-axis of the dq reference frame with $\overrightarrow{v}_{\mathrm{abc}_3}$, which is obtained by adding $\overrightarrow{v}_{\mathrm{a}_3\mathrm{o}}$, $\overrightarrow{v}_{\mathrm{b}_3\mathrm{o}}$, and $\overrightarrow{v}_{\mathrm{c}_3\mathrm{o}}$, it has $v_{\mathrm{d}_3} = v_{\mathrm{abc}_3}$ and $v_{\mathrm{q}_3} = 0$. Expressions of the active and reactive power transferred to the AC sub-grid can be rewritten as $P = v_{\mathrm{d}_3}i_{\mathrm{d}}$ and $Q = -v_{\mathrm{d}_3}i_{\mathrm{q}}$. Therefore, references for the d- and q-axis current can be obtained as $i_{\mathrm{d\_ref}} = \frac{P_{\mathrm{ref}}}{v_{\mathrm{d}_3}}$ and $i_{\mathrm{q\_ref}} = -\frac{Q_{\mathrm{ref}}}{v_{\mathrm{d}_3}}$, which are implemented in the vector control system presented in Fig. 3 (a). In the cases where the voltage of the DC sub-grid connected with bridge 1 and bridge 2 are of the same magnitude, the voltage outputs of bridge 1 and bridge 2 have the same magnitude and reverse phase.

2. *Vector Control System for Topology-B:* Fig 3 (b) shows the vector control system designed based on (10) for OETPT with Topology-B. Compared with that for Topology-A, different feed-forward compensation terms are applied. For the controller of bridge 1, feed-forward compensation terms are $v_{\mathrm{d}_3} - v_{\mathrm{d}_2} + 2R_{\mathrm{s}}i_{\mathrm{d}} - 2\omega_{\mathrm{s}}L_{\mathrm{s}}i_{\mathrm{q}}$ and $v_{\mathrm{q}_3} - v_{\mathrm{q}_2} + 2R_{\mathrm{s}}i_{\mathrm{q}} + 2\omega_{\mathrm{s}}L_{\mathrm{s}}i_{\mathrm{d}}$. For the controller of bridge 2, feed-forward compensation terms are $v_{\mathrm{d}_3} - v_{\mathrm{d}_1} + 2R_{\mathrm{s}}i_{\mathrm{d}} - 2\omega_{\mathrm{s}}L_{\mathrm{s}}i_{\mathrm{q}}$ and $v_{\mathrm{q}_3} - v_{\mathrm{q}_1} + 2R_{\mathrm{s}}i_{\mathrm{q}} + 2\omega_{\mathrm{s}}L_{\mathrm{s}}i_{\mathrm{d}}$. In Topology-B, control voltages of bridge 1 and bridge 2 are in the same phase.

The active power reference of controllers can be generated by frequency-droop or DC voltage-droop controllers, and the reactive power reference of controllers can be generated by AC voltage-droop controllers in practical situation. The existing techniques, which allow autonomous power flow between AC and DC sub-grids and regulate DC voltage and AC frequency, have been reviewed in Section 1. The focus of this paper is not on the stability control, namely, the frequency stability of AC sub-grids or the voltage stability of DC sub-grids, of hybrid micro-grids. Instead, the main contribution of this paper is proposing

two kinds of novel topologies for the interfaces between AC sub-grids and DC sub-grids. The proposed Topology-A and Topology-B not only inherit the simple structure and voltage transformation and current isolation capabilities of a conventional interface, but also possess the power flow control and power quality regulation functions of a solid state transformer-based interface. Hence, the proposed OETPT fills the gap between the conventional interface and the solid state transformer-based interface. Meanwhile, the OETPT requires only half number of transformers compared with the conventional interface, which significantly reduces the cost of a hybrid micro-grid.

IV. Simulation Results

OETPT and its control systems were tested with simulation studies through Matlab/Simulink here. The simulation step-length was set as 5 μs, and the sampling time of control systems was 50 μs.

TABLE I
PARAMETERS OF OETPT WITH TOPOLOGY-A

Parameter	Value	Parameter	Value
$P_{\rm n}$	2 MW	$f_{\rm n}$	50 Hz
$V_{\rm ns}$	11 kV	$V_{\rm np}$	2250 V
$L_{\rm l}$	0.06 p.u.	$R_{\rm l}$	0.002 p.u.
$L_{\rm m}$	200 p.u.	$R_{\rm m}$	200 p.u.
R	1×10^{-3} p.u.	L	0.1 p.u.
$V_{\rm dc\_nom}$	2400 V		

A. Case A: OETPT with Topology-A

Parameters of OETPT with Topology-A are presented in Table I, where $P_{\rm n}$ denotes the nominal power of OETPT, $f_{\rm n}$ is the nominal frequency of the AC sub-grid, $V_{\rm ns}$ represents the nominal line-to-line (LL) voltage of the secondary-side of OETPT, $V_{\rm np}$ is the nominal LL voltage of the primary-side of OETPT, and $V_{\rm dc\_nom}$ is the nominal voltage of the DC sub-grid.

Before $t = 0.4$ s, $P_{\rm ref} = 0$ W and $Q_{\rm ref} = -1$ MVar. At $t = 0.4$ s, the active power output reference stepped to 1 MW. The active power transferred to the AC sub-grid is illustrated in Fig. 4 (a), half of which was supplied by bridge 1, as presented in Fig. 4 (c). At $t = 0.6$ s, the reactive power reference jumped from -1 MVar to 1 MVar. The reactive power transferred to the AC sub-grid is shown in Fig. 4 (b), and half of the reactive power was supplied by bridge 1, as depicted in Fig. 4 (d).

In order to investigate the power control performance of Topology-A under unbalanced grid conditions, 0.2 p.u. and 0.15 p.u. negative sequence voltage components were added to the voltage of phase A and phase B of the voltage source of the AC sub-grid, respectively. The three-phase voltages of the AC sub-grid are presented in Fig. 4 (e). The active and reactive power commands were the same as those of normal operation condition. In this case, three-phase currents measured at the primary windings are unbalance as depicted in Fig. 4 (f). Nevertheless, the unbalanced operation conditions did not influence the power flow control performance. As illustrated in Fig. 4 (g) and Fig. 4 (h), the active power and reactive power transferred to the AC sub-grid can still follow the power commands, which can be explained as follows.

As presented in Fig. 2 (a) and Fig. 3 (a), the voltage compensation terms of the vector control system of OETPT with Topology-A are based on the measurement of the voltages of the AC sub-grid, i.e., $v_{\rm abc_3}$. Meanwhile, the vector control system uses AC voltage-oriented reference frame, and the phase angle of $v_{\rm abc_3}$ is adopted as the phase angle reference of the rotational reference frame of the control system. Therefore, the unbalance of AC sub-grid voltage can be fully sensed by the control systems of bridge 1 and bridge 2, and thus proper compensation voltages are generated by the control system. Consequently, the voltage unbalance of the AC sub-grid does not influence the active power and reactive power tracking performances of the OETPT.

Moreover, the voltage commands generated by the control system of converter 1 and converter 2 have the same magnitude and opposite phase as depicted in Fig. 3 (a). Therefore, converter 1 and converter 2 have symmetrical control voltages, and the control voltages are able to compensate with each other at all operating conditions. Thus the power sharing performances of the two converters are not influenced by the unbalanced AC sub-grid conditions as well.

Moreover, the power flow control performance of Topology-A was studied under fault conditions. A three-phase-to-ground fault was applied on the AC sub-grid at t =0.7167 s and the fault was cleared at $t = 0.7833$ s. The three-phase voltages measured at the terminals of the secondary windings of OETPT are illustrated with Fig. 4 (i). The three-phase currents of the primary windings are shown in Fig. 4 (j). Despite of the fault, the active and reactive power flow control of the OETPT still worked normally. According to Fig. 4 (k) and Fig. 4 (l), the active and reactive power outputs of bridge 1 stabilized to their referenced values respectively after some oscillations during the post-fault process.

B. Case B: OETPT with Topology-B

Parameters of OETPT with Topology-B are shown in Table II. Before $t = 0.4$ s, $P_{\rm ref} = 0$ W and $Q_{\rm ref} = 0$ Var. At $t = 0.4$, the active power reference stepped to -3.9 MW, and the AC sub-grid transferred 3.9 MW active power to the DC sub-grid, as

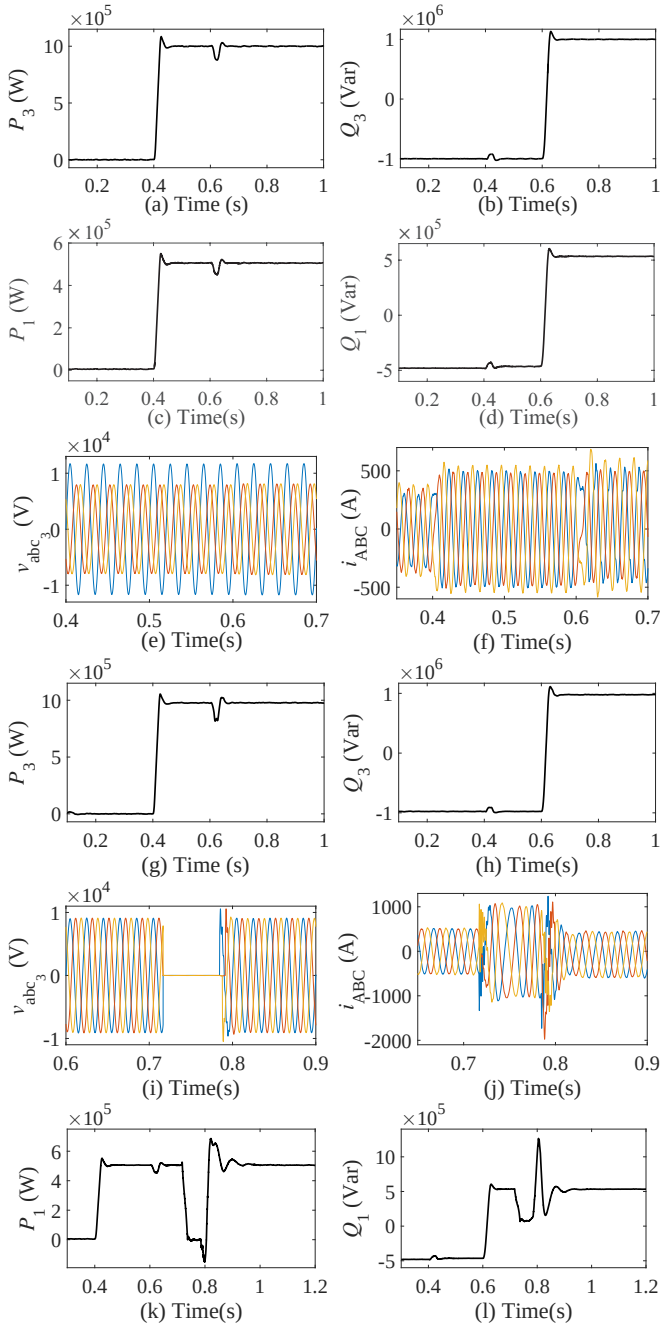

Fig. 4. Power flow control performance of OETPT with Topology-A ((a) Active power transferred to the AC sub-grid under normal operation condition (b) Reactive power transferred to the AC sub-grid under normal operation condition (c) Active power output of bridge 1 under normal operation condition (d) Reactive power output of bridge 1 under normal operation condition (e) Three-phase voltages of the AC sub-grid under voltage unbalance condition (f) Three-phase currents of the primary windings under voltage unbalance condition (g) Active power transferred to the AC sub-grid under voltage unbalance condition (h) Reactive power transferred to the AC sub-grid under voltage unbalance condition (i) Three-phase voltages of the AC sub-grid under fault condition (j) Three-phase currents of the primary windings under fault condition (k) Active power output of bridge 1 under fault condition (l) Reactive power output of bridge 1 under fault condition).

shown in Fig. 5 (a). Bridge 1 and bridge 2 absorbed 1.95 MW active power, respectively, which are presented in Fig. 5 (b) and 5 (c), respectively. At $t = 0.6$ s, the reactive power reference jumped to -2.36 MVar. The reactive power transmitted from the AC sub-grid to the DC sub-grid is depicted in Fig. 5 (d).

With the same active and reactive power control commands, the dynamics of OETPT was studied under voltage unbalance condition as well. 0.2 p.u. and 0.15 p.u. negative sequence voltage components were added to phase A and phase B of the voltage source of the AC sub-grid, respectively. Fig. 5 (e) depicts the three-phase voltage measured on the secondary windings. The active power transferred to the AC sub-grid and that generated by bridge 2 was able to track the active power control commands as shown in Fig. 5 (g) and Fig. 5 (h) despite of the unbalanced voltage of the AC sub-grid. Three-phase currents

TABLE II
PARAMETERS OF OETPT WITH TOPOLOGY-B

Parameter	Value	Parameter	Value
P_{n}	5 MW	f_{n}	50 Hz
V_{ns}	11 kV	V_{np}	11 kV
L_{l}	0.06 p.u.	R_{l}	0.002 p.u.
L_{m}	200 p.u.	R_{m}	200 p.u.
R	1×10^{-3} p.u.	L	0.1 p.u.
$V_{\mathrm{dc\_nom}}$	11 kV		

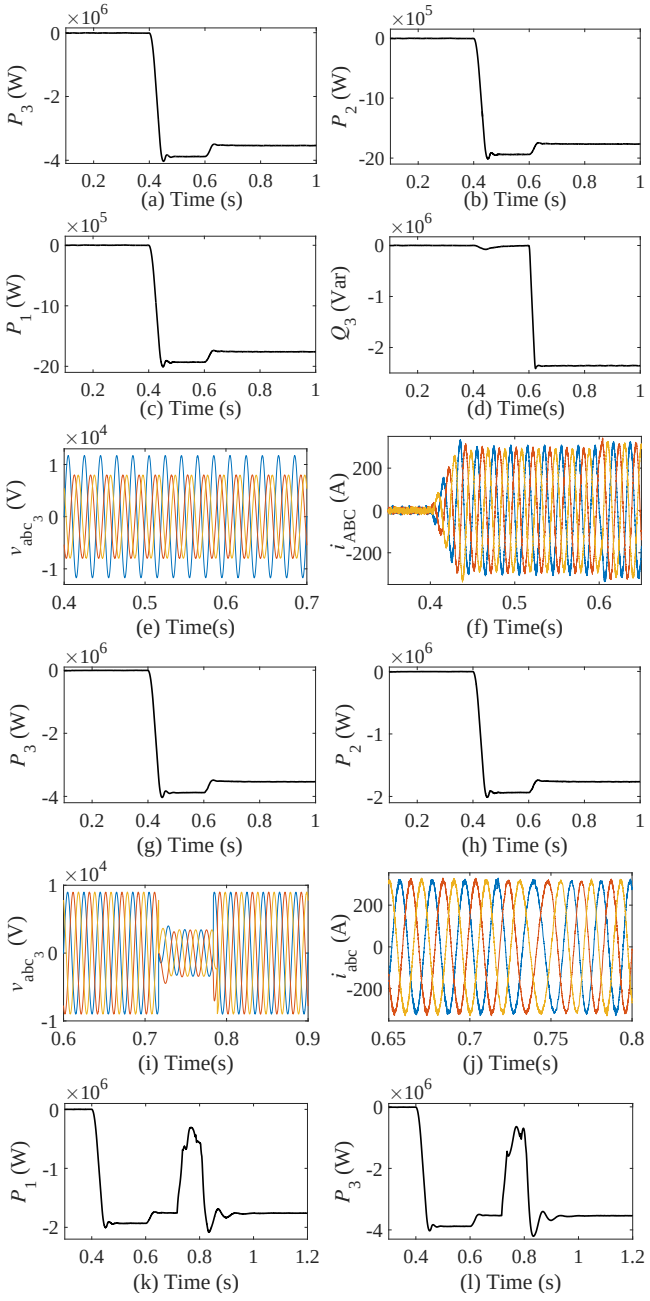

Fig. 5. Power flow control performance of OETPT with Topology-B ((a) Active power transferred to the AC sub-grid under normal operation condition (b) Active power output of bridge 2 under normal operation condition (c) Active power output of bridge 1 under normal operation condition (d) Reactive power transferred to the AC sub-grid under normal operation condition (e) Three-phase voltages of the AC sub-grid under voltage unbalance condition (f) Three-phase currents of the primary windings under voltage unbalance condition (g) Active power transferred to the AC sub-grid under voltage unbalance condition (h) Active power output of bridge 2 under voltage unbalance condition (i) Three-phase voltages of the AC sub-grid under fault condition (j) Three-phase currents of the secondary windings under fault condition (k) Active power output of bridge 1 under fault condition (l) Active power transferred to the AC sub-grid under fault condition).

of the primary windings presented small degree of unbalance, as illustrated in Fig. 5 (f).

Topology-B of OETPT was tested under fault condition as well. A three-phase-to-ground fault was applied on the AC sub-

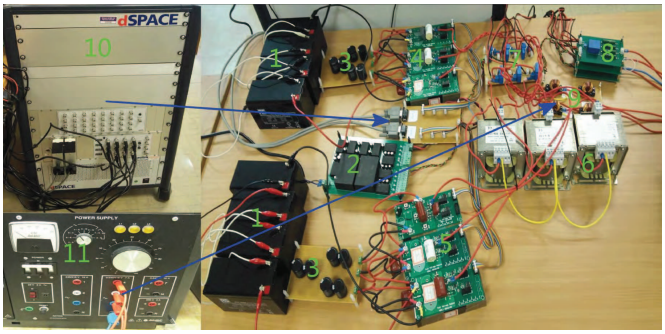

Fig. 6. Experimental platform (1. Batteries; 2. Auxiliary power source for converters; 3. Bus capacitors of converters; 4. Two-level bridge 1; 5. Two-level bridge 2; 6. Transformers with turns ratio of 1:1; 7. Current sensors; 8. Voltage sensors 9. Filters; 10. dSPACE; 11. AC power source for OETPT).

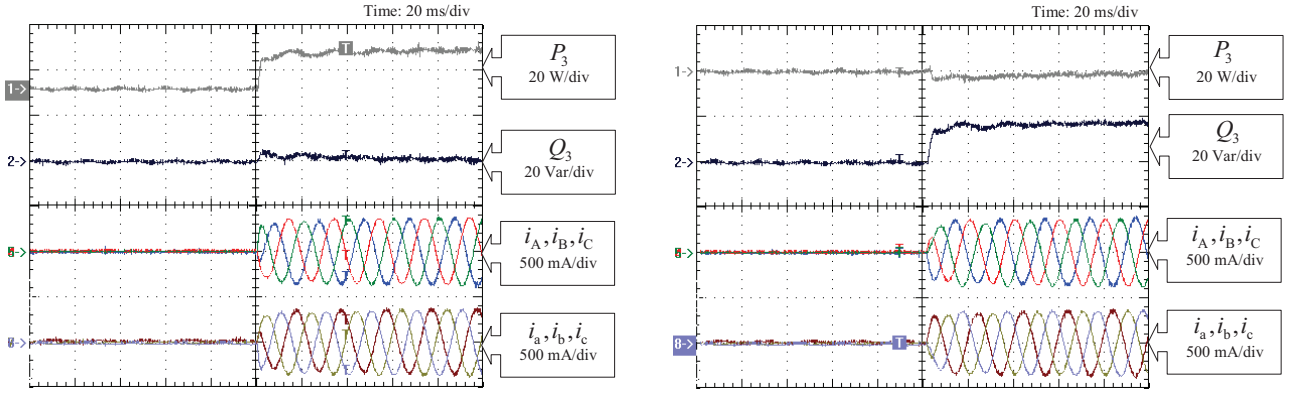

(a) Case 1: Active power reference P_{ref} stepped from 0 W to 40 W, and reactive power reference $Q_{\text{ref}} = 0$ Var.

(b) Case 2: Active power reference $P_{\text{ref}} = 0$ W, and reactive power reference Q_{ref} stepped from 0 Var to 40 Var.

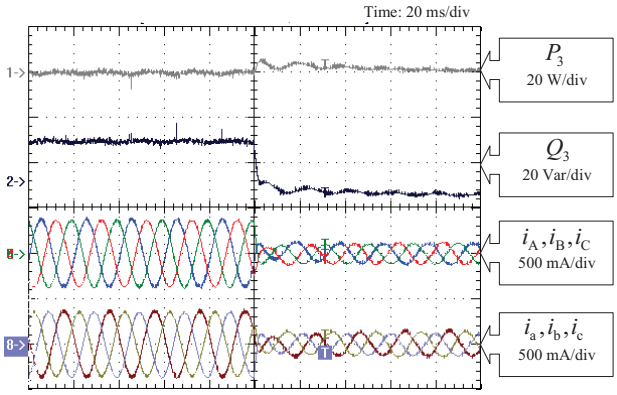

(c) Case 3: Active power reference $P_{\text{ref}} = 0$ W, and reactive power reference Q_{ref} stepped from 40 Var to -10 Var.

Fig. 7. Power flow control performance of OETPT with Topology-A.

grid at t =0.7167 s and cleared at $t = 0.7833$. The three-phase voltages measured out of the secondary windings are shown in Fig. 5 (i), and the three-phase currents of the secondary windings are presented in Fig. 5 (j). Due to the voltage disturbance, the active power generated by bridge 1 and that transmitted to the AC sub-grid stabilized to their desired values after some fluctuation, as shown in Fig. 5 (k) and Fig. 5 (l), respectively. Hence, Topology-B of OETPT is able to provide satisfactory power flow control performance under fault condition as well.

V. Experiment Results

The setup of the experiment platform is illustrated in Fig. 6. Components 2-9 constitute OETPT. The DC sub-grids of OETPT were modelled with two battery sets with terminal voltage of 50.6 V, i.e., component 1 presented in Fig. 6. The AC sub-grid of OETPT was modelled with a 50 Hz 26.5 V AC source presented as component 11 in Fig. 6. The control system of OETPT was implemented on a dSPACE illustrated as component 10 in Fig. 6. The sampling frequency of the control system was 5 kHz. The turns ratio of the three single-phase transformers was 1:1.

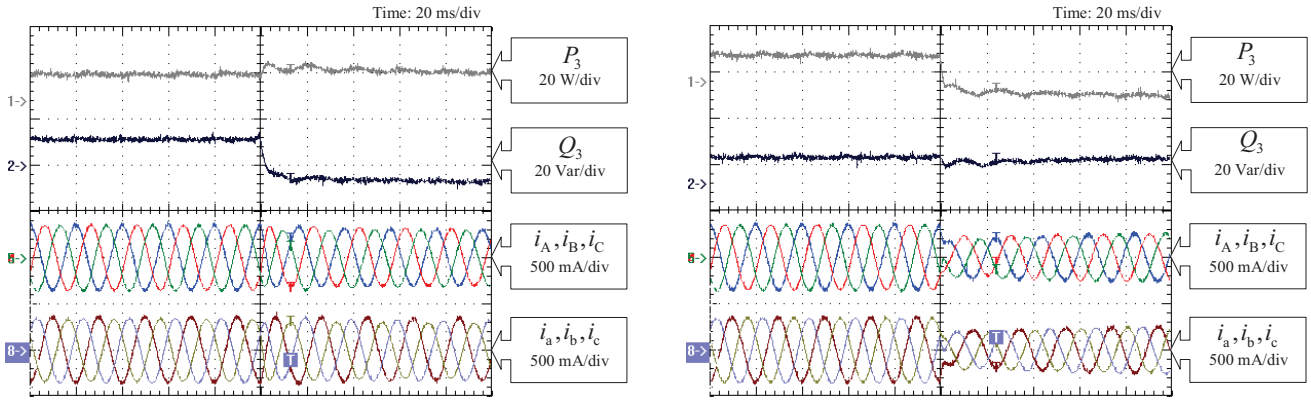

(a) Case 4: Active power reference $P_{\mathrm{ref}} = 30$ W, and reactive power reference Q_{ref} stepped from 30 Var to -18 Var.

(b) Case 5: Active power reference P_{ref} stepped from 30 W to -15 W, and reactive power reference $Q_{\mathrm{ref}} = 30$ Var.

Fig. 8. Power flow control performance of OETPT with Topology-A.

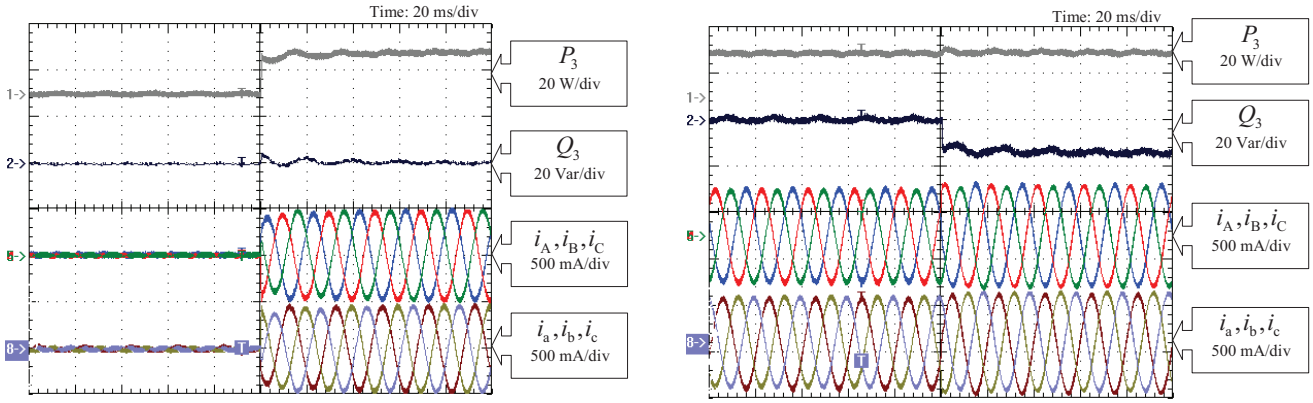

(a) Case 1: Active power reference P_{ref} stepped from 0 W to 18 W, and reactive power reference $Q_{\mathrm{ref}} = 0$ Var.

(b) Case 2: Active power reference $P_{\mathrm{ref}} = 18$ W, and reactive power reference Q_{ref} stepped from 0 Var to -7.2 Var.

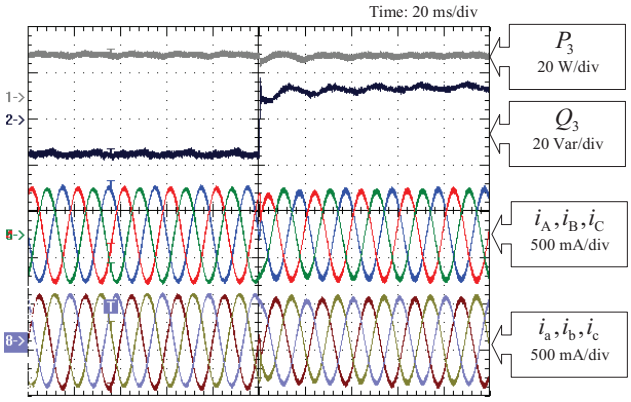

(c) Case 3: Active power reference $P_{\mathrm{ref}} = 18$ W, and reactive power reference Q_{ref} stepped from -7.2 Var to 7.2 Var.

Fig. 9. Power flow control performance of OETPT with Topology-B.

A. Power Flow Control Performance of OETPT with Topology-A

Five cases were tested on the experiment platform, which covered the bidirectional transmission of active and reactive power between the AC sub-grid and DC sub-grid of OETPT with Topology-A. Specifically, in case 1, the active power reference P_{ref} stepped from 0 W to 40 W, and the reactive power reference Q_{ref} was maintained at 0 Var. The dynamics of the active power P_3 and reactive power Q_3 transmitted to the AC sub-grid are illustrated in Fig. 7 (a), where the three-phase current i_{ABC} (abbreviation for i_{A}, i_{B}, and i_{C}) measured at the primary-side of the transformer and i_{abc} (abbreviation for i_{a}, i_{b}, and i_{c}) measured at the secondary-side of the transformer are presented as well.

In case 2, P_{ref} was kept at 0 W, and Q_{ref} stepped from 0 Var to 40 Var. The DC sub-grid transmitted pure reactive power to the AC sub-grid. The dynamics of P_3, Q_3, i_{ABC}, and i_{abc} are presented in Fig. 7 (b). The dynamics of P_3, Q_3, i_{ABC},

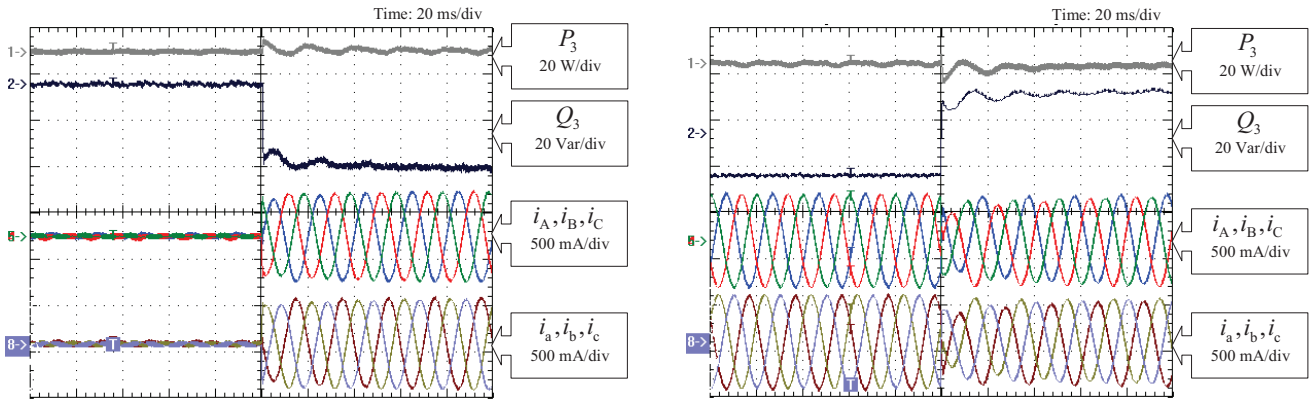

(a) Case 4: Active power reference $P_{\rm ref} = 0$ W, and reactive power reference $Q_{\rm ref}$ stepped from 0 Var to -18 Var.

(b) Case 5: Active power reference $P_{\rm ref} = 0$ W, and reactive power reference $Q_{\rm ref}$ stepped from -18 Var to 18 Var.

Fig. 10. Power flow control performance of OETPT with Topology-B.

and $i_{\rm abc}$ obtained in the case, where $P_{\rm ref}$ was kept at 0 W and $Q_{\rm ref}$ was reduced from 40 Var to -10 Var, are illustrated as case 3 in Fig. 7 (c). In this case, the change of reactive power transmission direction was tested. In case 4, OETPT was controlled to transmit active and reactive power simultaneously, and the change of reactive power transmission direction was tested. Specifically, $P_{\rm ref}$ was regulated at 30 W and $Q_{\rm ref}$ jumped from 30 Var to -18 Var. The dynamics of P_3, Q_3, $i_{\rm ABC}$, and $i_{\rm abc}$ are shown in Fig. 8 (a). It can be observed that the change of reactive power direction was accompanied by a variation of the phase angle of three-phase current. The step change of active power was tested in case 5, where $P_{\rm ref}$ jumped from 30 W to -15 W and $Q_{\rm ref}$ was kept at 30 Var. The dynamics of P_3, Q_3, $i_{\rm ABC}$, and $i_{\rm abc}$ are illustrated in Fig. 8 (b). According to the results presented in Fig. 7 and 8, it manifests that OETPT with Topology-A is able to realize the decoupled control of active and reactive power transmitted between the AC sub-grid and the DC sub-grid.

B. Power Flow Control Performance of OETPT with Topology-B

In this section, the power flow control performance of OETPT with Topology-B was tested on the experiment platform in another five cases.

In case 1, $P_{\rm ref}$ stepped from 0 W to 18 W and $Q_{\rm ref}$ maintained at 0 Var. The DC sub-grid transmitted pure active power to the AC sub-grid. The dynamics of P_3, Q_3, $i_{\rm ABC}$, and $i_{\rm abc}$ are illustrated in Fig. 9 (a). The step change of reactive power was tested in case 2, where $P_{\rm ref}$ was kept at 18 W and $Q_{\rm ref}$ jumped from 0 Var to -7.2 Var. The dynamics of P_3, Q_3, $i_{\rm ABC}$, and $i_{\rm abc}$ are presented in Fig. 9 (b). In case 3, $P_{\rm ref}$ maintained at 18 W and $Q_{\rm ref}$ jumped from -7.2 Var to 7.2 Var. The dynamics of P_3, Q_3, $i_{\rm ABC}$, and $i_{\rm abc}$ are shown in Fig. 9 (c). With $P_{\rm ref}$ fixed at 0 W, $Q_{\rm ref}$ stepped from 0 Var to -18 Var in case 4. The AC sub-grid transmitted pure reactive power to the DC sub-grid, and Fig. 10 (a) depicts the dynamics of P_3, Q_3, $i_{\rm ABC}$, and $i_{\rm abc}$. In case 5, $P_{\rm ref}$ was fixed at 0 W and $Q_{\rm ref}$ stepped from -18 Var to 18 Var. The AC sub-grid exchanged pure reactive power with the DC sub-grid and the bidirectional reactive power transmission was tested. The dynamics of P_3, Q_3, $i_{\rm ABC}$, and $i_{\rm abc}$ are shown in Fig. 10 (b).

VI. Discussions

The main contribution of this paper is to explore the flexible power flow control capability of OETPT. The impacts of the active and reactive power flows on the DC sub-grid voltage and AC sub-grid frequency are not the focus here. However, the regulation of DC sub-grid voltage and AC sub-grid frequency can be realized with additional DC voltage and AC frequency droop control loops, which has been widely investigated in the existing studies, such as [35],[36]. Therefore, the impact of the power flows on the DC sub-grid voltage and AC sub-grid frequency were not investigated in this paper. Out of the perspective of OETPT, the converters of OETPT actually belong to the AC sub-grid of the system, thus the reactive power control configuration of the control scheme facilitates the voltage regulation of the AC sub-grid with additional droop controllers.

According to the simulation and experimental results, both the OETPTs with Topology-A and Topology-B are able to achieve flexible power flow control under all the tested operating conditions. Compared with Topology-B, Topology-A suits for a wider voltage levels of AC sub-grids and DC sub-grids. The control system of Topology-A has simpler structure than that of Topology-B. Topology-B is preferred when the grounding point is desirable at the primary-side of the transformer.

VII. Conclusions

This paper has proposed an OETPT for the interconnection of the AC sub-grid and the DC sub-grid of a hybrid micro-grid. OETPT is constructed with the off-the-shelf components of the conventional AC/DC interface of a hybrid micro-gird, and it offers flexible power flow control capability.

Two topologies, in which primary or secondary windings of OETPT are grounded respectively, were designed. According to the steady-state equivalent circuit analysis, the regulation of the active and reactive power flowing between the AC sub-grid and the DC sub-grid can be realized with an integrated control of two two-level bridges of OETPT. A vector control system was designed for the coordinated control of OETPT with Topology-A and Topology-B, respectively.

Referring to simulation results, both OETPTs with Topology-A and Topology-B are able to achieve the decoupled active and reactive power control. OETPT with Topology-B suits for the inter-connection of AC and DC micro-grids in similar voltage levels, such as the case of 11 kV AC and 11 kV DC presented in simulation studies. By contrast, OETPT with Topology-A can be used for the interconnection of AC and DC micro-grids with arbitrary practical voltage levels. Topology-B is the priority when grounding point is required at the primary-side of OETPT. Moreover, both OETPTs with Topology-A and Topology-B are able to provide satisfactory power flow control performance under grid unbalance operation conditions. They are also robust to severe grid faults, such as three-phase-to-ground faults occurred on the AC sub-grid. During the fault processes, the exchange of active and reactive powers between the AC sub-grid and the DC sub-grid is obstructed. The power exchange can be recovered with slight oscillations, which verifies the robustness of the control systems designed for Topology-A and Topology-B. Experiment results further verify that both Topology-A and Topology-B of OETPT are able to realize the bidirectional decoupled control of active and reactive powers.

VIII. Acknowledgements

This work was supported in part by the State Key Program of National Science of China under Grant 51437006, Project funded by China Postdoctoral Science Foundation under Grant 2017M620373, Guangdong Innovative Research Team Program under Grant 201001N0104744201, and China Scholarship Council.

IX. References

[1] N. Eghtedarpour, E. Farjah: 'Power control and management in a hybrid AC/DC microgrid', IEEE Trans. Smart Grid, 2014, 5, (3), pp. 1494–1505

[2] J. M. Guerrero, M. Chandorkar, T. L. Lee, et al.:'Advanced control architectures for intelligent microgrids–part I: Decentralized and hierarchical control', IEEE Trans. Ind. Electron., 2013, 60, (4), pp 1254–1262

[3] D. Dong, T. Thacker, I. Cvetkovic, et al.:'Modes of operation and system-level control of single-phase bidirectional PWM converter for microgrid systems', IEEE Trans. Smart Grid, 2012, 3, (1), pp 93–104

[4] X. Lu, J. M. Guerrero, K. Sun, et al.:'Hierarchical control of parallel AC-DC converter interfaces for hybrid microgrids', IEEE Trans. Smart Grid, 2014, 5, (2), pp 683–692

[5] Y. Hu, J. Zhang, J. Wu, et al.:'Efficiency improvement of nonuniformly aged PV arrays', IEEE Trans. Power Electron., 2017, 32, (2), pp 1124–1137

[6] H. R. Baghaee, M. Mirsalim, G. B. Gharehpetian, et al.:'A decentralized power management and sliding mode control strategy for hybrid AC/DC microgrids including renewable energy resources', IEEE Trans. Ind. Inform., 2017, PP, (99), pp 1–1

[7] K. Sun, X. Wang, Y. W. Li, et al.:'Parallel operation of bi-directional interfacing converters in a hybrid AC/DC microgrid under unbalanced grid voltage conditions', IEEE Trans. Power Electron., 2017, 32, (3), pp 1872–1884

[8] P. Wang, C. Jin, D. Zhu, et al.:'Distributed control for autonomous operation of a three-port AC/DC/DS hybrid microgrid', IEEE Trans. Ind. Electron., 2015, 62, (2), pp 1279–1290

[9] J. He, Y. W. Li, D. Bosnjak, et al.:'Investigation and active damping of multiple resonances in a parallel-inverter-based microgrid', IEEE Trans. Power Electron., 2013, 28, (1), pp 234–246

[10] J. He, Y. W. Li, J. M. Guerrero, et al.:'An islanding microgrid power sharing approach using enhanced virtual impedance control scheme', IEEE Trans. Power Electron., 2013, 28, (11), pp 5272–5282

[11] J. He, Y. W. Li, F. Blaabjerg, et al.:'Flexible microgrid power quality enhancement using adaptive hybrid voltage and current controller', IEEE Trans. Ind. Electron., 2014, 61, (1), pp 2784-2794

[12] H. Qin, J. W. Kimball:'Solid-state transformer architecture using AC-AC dual-active-bridge converter', IEEE Trans. Ind. Electron., 2013, 60, (9), pp 3720–3730

[13] Y. Hu, J. Wu, W. Cao, et al:'Ultrahigh step-up DC/DC converter for distributed generation by three degrees of freedom (3DoF) approach', IEEE Trans. Power Electron., 2016, 31, (7), pp 4930-4941

[14] Y. Hu, C. Gan, W. Cao, et al:'Flexible fault-tolerant topology for switched reluctance motor drives', IEEE Trans. Power Electron., 2016, 31, (6), pp 4654-4668

[15] William Mcmurray: 'Power converter circuits having a high frequency link', US Patent 3,517,300, Jun 1970

[16] M. Kang, P. N. Enjeti, I. J. Pitel:'Analysis and design of electronic transformers for electric power distribution system', IEEE Trans. Power Electron., 1999, 14, (6), pp 1133–1141

[17] B. Zhao, Q. Song, W. Liu:'A practical solution of high-frequency-link bidirectional solid-state transformer based on advanced components in hybrid microgrid', IEEE Trans. Ind. Electron., 2015, 62, (7), pp 4587–4597

[18] Falcones Sixifo, Ayyanar Rajapandian, Mao, Xiaolin:'A DC–DC multiport-converter-based solid-state transformer integrating distributed generation and storage', IEEE Trans. Power Electron., 2013, 28, (5), pp 2192–2203

[19] Falcones Sixifo, Ayyanar Rajapandian, Mao, Xiaolin:'A DC–DC multiport-converter-based solid-state transformer integrating distributed generation and storage', IEEE Trans. Power Electron., 2013, 28, (5), pp 2192–2203

[20] G. Wang, X. Huang, J. Wang, et al:'Comparisons of 6.5kV 25 A Si IGBT and 10kV SiC MOSFET in solid-state transformer application', 2010 IEEE Energy Conversion Congress and Exposition, Sep. 2010, pp 100–104

[21] P. C. Loh, D. Li, Y. K. Chai, et al:'Autonomous control of interlinking converter with energy storage in hybrid ac-dc microgrid', IEEE Trans. Ind. Appl., 2013, 49 (3), pp 1374–1382

[22] A. Abdelsalam, H. Gabbar, A. Sharaf:'Performance enhancement of hybrid ac/dc microgrid based d-facts', Int. J. Elect. Power and Energy Syst., 2014, 63, pp 382–393

[23] A. A. A. Radwan, Y. A. R. I. Mohamed:'Assessment and mitigation of interaction dynamics in hybrid ac/dc distribution generation systems', IEEE Trans. Smart Grid, 20112, 3 (3), pp 1382–1393

[24] G. Gohil, L. Bede, R. Teodorescu, et al:'Dual converter fed open-end transformer topology with parallel converters and integrated magnetics', IEEE Trans. Ind. Electron., 2016, 63, (8), pp 4929–4941

[25] G. Gohil, L. Bede, R. Teodorescu, et al:'Optimized integrated harmonic filter inductor for dual-converter fed open-end transformer topology', IEEE Trans. Ind. Electron., 2016, PP, (99), pp 1–1

[26] H. Han, X. Hou, J. Yang, et al:'Review of power sharing control strategies for islanding operation of ac microgrids', IEEE Trans. Smart Grid, 2016, 7 (1), pp 200–215

[27] Q. Xu, J. Xiao, X. Hu, et al:'A decentralized power management strategy for hybrid energy storage system with autonomous bus voltage restoration and state-of-charge recovery', IEEE Trans. Ind. Electron., 2017, 64 (9), pp 7098–7108

[28] H. Xiao, A. Luo, Z. Shuai, et al:'An improved control method for multiple bidirectional power converters in hybrid AC/DC microgrids', IEEE Trans. Smart Grid, 2016, 7 (1), pp 340–347

[29] Y. Shi, W. Wu, H. Wang, et al:'The parallel multi-inverter system based on the voltage-type droop control method', IEEE J. Em. Sel. Top. P., 2016, 4 (4), pp 1332–1341

[30] L. Lin, H. Ma, Z. Bai:'An improved proportional load-sharing strategy for meshed parallel inverters system with complex impedances', IEEE Trans. Power Electron., 2017, 32 (9), pp 7338–7351

[31] J. Liu, Y. Miura, H. Bevrani, et al:'Enhanced virtual synchronous generator control for parallel inverters in microgrids', IEEE Trans. Smart Grid, 2017, 8 (5), pp 2268–2277

[32] Y. Xia, Y. Peng, P. Yang, et al:'Distributed coordination control for multiple bidirectional power converters in a hybrid ac/dc mirogrid', IEEE Trans. Power Electron., 2017, 32 (6), pp 4949–4959

[33] P. Kundur, N. J. Balu, M.G. Lauby:'Power system stability and control', McGraw-hill New York, 1994, vol. 7

[34] Y. Liu, Q. H. Wu, X. X. Zhou:'Co-ordinated multiloop switching control of DFIG for resilience enhancement of wind power penetrated power systems', IEEE Trans. Sustain. Energy, 2016, 7, (3), pp 1089–1099

[35] Qobad Shafiee, Josep M. Guerrero, Juan C. Vasquez:'Distributed secondary control for islanded microgirds-A novel approach', IEEE Trans. Power Electron., 2014, 29, (2), pp 1018–1031

[36] Sijo Augustine, N. Lakshminarasamma, Mahesh Kumar Mishra:'Control of photovoltaic-based low-voltage dc microgrid system for power sharing with modified droop algorithm', IET Power Electron., 2016, 9, (6), pp 1132–1143